Stability of Hierarchical Lamellar Morphologies Formed in ABC Star Triblock Copolymers

YUCI XU,[1] WEIHUA LI,[1] FENG QIU,[1] HONGDONG ZHANG,[1] YULIANG YANG,[1] AN-CHANG SHI[2]

[1]Department of Macromolecular Science, The Key Laboratory of Molecular Engineering of Polymers, Ministry of Education, Fudan University, Shanghai 200433, China

[2]Department of Physics and Astronomy, McMaster University, Hamilton, Ontario, Canada L8S 4M1

Received 22 November 2009; revised 3 February 2010; accepted 17 February 2010
DOI: 10.1002/polb.22000
Published online in Wiley InterScience (www.interscience.wiley.com).

ABSTRACT: The stability of hierarchical lamellar morphologies formed in ABC star triblock copolymers, is studied using the self-consistent mean-field theory. The hierarchical lamellae consist of repeating period of the largest block A-formed layer and B/C coformed layer where B and C domains are arranged alternatively. An angle, which is used to characterize the shifting magnitude between two neighbor B/C coformed layers, varies from 0 to 180 degrees. By comparing the free energy among the lamellar morphologies with various shift angle, their relative stability is analyzed. Our results show that the morphology with larger shift has lower entropic energy and higher internal energy. In general, the morphology with the largest shift of 180-degree is stable compared with those with smaller shift as the entropic energy dominates the internal energy. However, the relative stability can be tuned by the interactions among the three components as well as their relative compositions. PACS numbers: 61.25.Hq, 64.60.Cn, 64.75.+g. © 2010 Wiley Periodicals, Inc. J Polym Sci Part B: Polym Phys 48: 1101–1109, 2010

KEYWORDS: phase behavior; self-assembly; theory

INTRODUCTION Block copolymers have attracted a lot of attentions due to their ability to self-assemble into rich nanoscale ordered morphologies. This property make them candidates for wide potential applications including lithographic templates for nanowires, photonic crystals, and high density magnetic storage media.[1] As the simplest model of block copolymers, diblock copolymer has been extensively studied both by experiments[2–4] and by theories.[5–8] There are two factors influencing the phase separation of diblock copolymers: the composition f of one species and the product χN of the polymerization N and the Flory-Huggins parameter χ which characterizes the interaction between dissimilar monomers. Because of its simplicity, its self-assembling behavior have been understood well. The classical mesophases formed by diblock copolymers include lamellae, cylinders, spheres and gyroid.[6] In addition, O^{70} phase (*Fddd*, orthorhombic network) is determined as a stable phase with a small region surrounded by cylinder, gyroid, and lamellar phases.[9,10]

With the development of synthesizing techniques, it is possible to make more complex block copolymers through different methods. One way is to add more chemical components into the copolymer, another way is to add more blocks onto the chain without introducing new components (such as two-component ABA triblock copolymer), and the third way is to control the architecture of the chain for multiblock copolymers. For example, adding a block composed of a new component of C onto an AB diblock copolymer chain leads to ABC triblock copolymers. Furthermore, there are many candidates of topological architectures: linear, star and so on. In the linear one, the three blocks have different aligning sequences. In the ABC star triblock copolymers, one end of each block is jointed together. For three-component block copolymers, a lot of possible multiblock copolymers can be synthesized by adding more blocks. The phase behaviors of ABC triblock copolymers are much more complicated than that of AB diblock copolymers. The parameters influencing the bulk phases increase from two to five including three interaction parameters $\chi_{AB}N$, $\chi_{AC}N$, $\chi_{BC}N$ and two independent volume fractions f_A and f_B. In another word, their phase diagrams become five dimensional. Exploring the whole phase diagrams in this parameter space is a formidable task. However, by varying the five parameters, many interesting ordered microstructures can be observed, or some two-dimensional phase diagrams can be explored by fixing three of the five parameters. The linear triblock copolymer melts are likely to form novel decorated phases, such as spheres on spheres, spheres on cylinders, rings on cylinders, and cylinders in lamellae, with $\chi_{AC} < \chi_{AB} < \chi_{BC}$; core-shell versions and alternating versions of those phases observed in diblock copolymers with $\chi_{AB} \leq \chi_{BC} < \chi_{AC}$; and phases spanning the range of phases between those in above two cases.[10]

Correspondence to: W. Li (E-mail: weihuali@fudan.edu.cn)
Journal of Polymer Science: Part B: Polymer Physics, Vol. 48, 1101–1109 (2010) © 2010 Wiley Periodicals, Inc.

The self-assembly of the star triblock copolymer melt is very different from that of the linear one. A lot of experiments have been done to study the formation of morphologies[11–23] since the first three-miktoarm star copolymers were synthesized in 1992 by Iatrou and Hadjichristidis[24] and by Fujimoto et al.[25] In 2002, a comparable systematical research was carried on the self-assembling of a series of ABC star copolymers of the type $A_xB_{1.0}C_{1.0}$ with a wide x range from about 0.2 to 25 using Monte Carlo simulations by Gemma et al.[26] They proposed that cylindrical phases of polygonal-tiling patterns, with the three-arm junctions aligning on a straight line, are formed when the three components are immiscible and the three arms are long enough to give stable three-phase structures. For x increasing from about 0.4 to 2.5, the sequence of these two-dimensional (2D) polygonal structures is [8.8.4], [6.6.6], [8.6.4:8.6.6], [10.6.4:10.6.4; 10.6.6], and [12.6.4] (these integer numbers indicate the side numbers of these polygons). These microstructures were observed in a serial experiments,[27] and some of them were seen in the dissipative particle dynamics simulations (DPD) by Huang et al.[28] When x is between 3 and 5, a structure of Lamella+Cylinder was observed. This structure can be seen as a hierarchical lamellar phase composed of A layer and B/C-layer, in which the B and C blocks further separate to form B/C repeating domains. Two lengths are required to characterize the structure: one is for the B/C domain repeating spacing (denoted as L_1), and the other is for the distance between two neighbor A layers (denoted as L_2).[29] This structure was also observed in ABC star copolymers with the ratios of the three arms 3 : 1 : 1 by Tang et al.;[30] and with three equal length arms and three different interactions by Wang and coworkers[31] and in the blends of ABC star copolymers and homopolymer by Liang's group.[32] In this hierarchical lamellae, two neighbor B/C-layers can have different ways of arrangement by varying the relative positions of B or C domains. In the Figure 12(b) of ref. 26 the B and C domains in two neighbor B/C-layers are arranged synchronously; however, they are arranged in the complementary position in ref. 30. For the former case, the shift of two neighbor B/C-layers is zero, and for the latter case, the shift is a half of the period of L_1. Both arrangements were seen in the work of Liang's group.[32] Two questions can be asked about these phenomena. Which arrangement of B/C domains is preferred by this hierarchical lamellar phase? And, can the stable morphology have other B/C domain arrangements besides the above two?

To answer these questions, we focus in the present work on the study of the stability of the hierarchical lamellar phase with different arrangements of B/C domains. We refer the shift of the arrangement to an angle varying from zero (none shift) to 180 degrees (the largest shift, or $L_1/2$ shift). Our study is carried out by using self-consistent mean-field theory (SCMFT) which is one of the most successful methods on the study of block copolymers[6,33,34] since it was applied to this field.[5,35,36] In particular, SCMFT can determine the relative stability of different phases because it can calculate the free energy accurately. According to the schemes of solving the modified diffusion equations of the propagators, a few methods have been developed. One of successful methods, the spectral method, is very successful on determining phase diagrams as it has high accuracies with free energy calculations when the symmetries of phases are known.[6] Very recently, Guo et al. have proposed a developed spectral method which can be used to look for new structures as the real-space method does.[37] This new spectral method requires many basis functions for accurate calculation of free energy. This restricts its application on the determination of phase diagram. Combining the developed spectral method with the tranditional spectral method may be a reasonable choice to determine phase diagram: the former is used to look for new structures and to determine the symmetries of found structures, and then the latter is used to calculate the free energy accurately of these structures with determined symmetries by the former. In the current study we apply another method, the real-space method proposed by Drolet and Fredrickson.[7] The pseudo-spectral scheme of real-space method, which is developed by Tzeremes et al.,[38,39] is used to solve the modified diffusion equations. This operator-split algorithm as a second-order method (OpS2) has high effieciency, and can be readily parallized by using FFTW package to do the fast-fourier transformations. The real-space method is convenient to obtain structures with varying shift for the hierarchical lamellae by using various initial conditions. However, confident accuracy of the free energy in the real-space method requires high-degree discretization on the chain contour length. Fortunately, a newly proposed fourth-order backward-differentiation-formula scheme (BDF4) based on the operator-split algorithm allows reasonable discretization ($\Delta s = 0.001$) for enough high accuracy of free energy.[40] We also use this BDF4 scheme as a reference to justify the reliability of our results obtained by OpS2.

THEORY

We consider an incompressible melt of ABC star triblock copolymers with a degree of polymerization N in a volume of V, and the chain lengths of A, B, and C blocks are f_AN, f_BN, and f_CN ($f_A + f_B + f_C = 1$), respectively. Spacial lengths in our calculations are expressed in units of the radius of gyration, R_g, of the polymer. Within the mean-field approximation to the many-chain Edwards theory,[34,35] at a temperature T, the free energy F for n Gaussian triblock copolymer chains

$$\frac{F}{nk_BT} = -\ln Q + \frac{1}{V}\int d\mathbf{r}\{\chi_{AB}N\phi_A(\mathbf{r})\phi_B(\mathbf{r}) + \chi_{AC}N\phi_A(\mathbf{r})\phi_C(\mathbf{r}) + \chi_{BC}N\phi_B(\mathbf{r})\phi_C(\mathbf{r}) - \omega_A(\mathbf{r})\phi_A(\mathbf{r}) - \omega_B(\mathbf{r})\phi_B(\mathbf{r}) - \omega_C(\mathbf{r})\phi_C(\mathbf{r}) - \eta(\mathbf{r})[1 - \phi_A(\mathbf{r}) - \phi_B(\mathbf{r}) - \phi_C(\mathbf{r})]\}. \quad (1)$$

where ϕ_A, ϕ_B, and ϕ_C are the monomer densities. The partition function Q is for a single polymer chain interacting with the mean fields ω_A, ω_B, and ω_C produced by the surrounding chains. The interactions among the three dissimilar monomers are characterized by three Flory-Huggins interaction parameters, χ_{AB}, χ_{AC}, and χ_{BC}. Minimization of the free energy with respect to the monomer densities and the mean fields leads to the following standard mean-field equations[34]

$$\omega_A(\mathbf{r}) = \chi_{AB}N\phi_B(\mathbf{r}) + \chi_{AC}N\phi_C(\mathbf{r}) + \eta(\mathbf{r})$$
$$\omega_B(\mathbf{r}) = \chi_{AB}N\phi_A(\mathbf{r}) + \chi_{BC}N\phi_C(\mathbf{r}) + \eta(\mathbf{r})$$
$$\omega_C(\mathbf{r}) = \chi_{AC}N\phi_A(\mathbf{r}) + \chi_{BC}N\phi_B(\mathbf{r}) + \eta(\mathbf{r})$$
$$\phi_A(\mathbf{r}) = \frac{1}{Q}\int_0^{f_A} ds\; q_A(\mathbf{r},s)q_A^\dagger(\mathbf{r},s)$$
$$\phi_B(\mathbf{r}) = \frac{1}{Q}\int_0^{f_B} ds\; q_B(\mathbf{r},s)q_B^\dagger(\mathbf{r},s)$$
$$\phi_C(\mathbf{r}) = \frac{1}{Q}\int_0^{f_C} ds\; q_C(\mathbf{r},s)q_C^\dagger(\mathbf{r},s)$$
$$Q = \frac{1}{V}\int d\mathbf{r}\; q_K(\mathbf{r},s)q_K^\dagger(\mathbf{r},s)$$
$$\phi_A(\mathbf{r}) + \phi_B(\mathbf{r}) + \phi_C(\mathbf{r}) = 1 \qquad (2)$$

In the above equations, $q_K(\mathbf{r},s)$ and $q_K^\dagger(\mathbf{r},s)$ (K = A, B, C) are end-segment distribution functions which have standard definitions.[34] These distribution functions satisfy the modified diffusion equations

$$\frac{\partial q_K(\mathbf{r},s)}{\partial s} = \nabla^2 q_K(\mathbf{r},s) - \omega_K(\mathbf{r},s)q_K(\mathbf{r},s) \qquad (3)$$
$$-\frac{\partial q_K^\dagger(\mathbf{r},s)}{\partial s} = \nabla^2 q_K^\dagger(\mathbf{r},s) - \omega_K(\mathbf{r},s)q_K^\dagger(\mathbf{r},s) \qquad (4)$$

The initial conditions are $q_K(\mathbf{r},0) = q_L^\dagger(\mathbf{r},0)q_M^\dagger(\mathbf{r},0)$, where (KLM) $\in$ {(ABC), (BCA), (CAB)}, and $q_K^\dagger(\mathbf{r},f_K) = 1$. For numerical solution, we employ the pseudo-spectral method[38,39] or the fourth-order implicit-explicit real-space method[40] to solve the modified diffusion equations for the end-segment distribution functions. In our calculations, the ABC star copolymer chains are put in a rectangle box with sizes of $L_x \times L_y$ as the considered hierarchical lamellar structure is two-dimensional, and the lamellae are aligned along one side of the box by using appropriate initial conditions. In the two real-space methods, periodic boundary conditions are imposed automatically on the two directions of the box. In our 2D SCMFT calculations, a lattice of $N_x \times N_y = 128 \times 128$ is used to discretize the space, and the chain contour length is divided into N_s points.

In this work, we first use various initial conditions to generate a set of hierarchical lamellae with varying shifts as solutions of the mean-field equations. Once we determine the set of structures, we then use these structures as initial conditions in our algorithm to obtain their free energy which is used to identify their stabilities.

RESULTS AND DISCUSSION

As our investigation focuses on a star triblock copolymer melt which forms hierarchical lamellar phase in the bulk, we choose its volume fractions as $f_A = 0.6$ and $f_B = f_C = 0.2$ in the whole work except for some places where specific illustrations are given, and we fix $\chi_{AB} = \chi_{AC}$ to give prominence to the main effects which influence the relative stability of these morphologies. The density profiles of nine typical hierarchical lamellae with varying shifts (0, 22.5, . . . , 180 degrees) are shown in Figure 1. Three colors of red, green, and blue, correspond to the phase regions where the main component is A, B, and C, respectively. Here the shift is characterized by a shift angle which is proportional to the magnitude of the shift. The zero-degree shift means that all of B/C layers have synchronous arrangements of B/C alternative domains, and the 180-degree shift means that two neighbor B/C layers have complemental arrangements. The morphologies of zero-shift and 180-degree-shift can be produced with random initial conditions, and the others are obtained by shifting one of every two B/C layers of the two known morphologies with a given shift. On this view, these morphologies with the shift angle between zero and 180 degrees are artificially made. Note that the basic units of the morphologies are not a parallelogram except for that of the 180-degree-shift one, but a rectangle. This is the reason that a rectangular box is used in our calculations. The discussion of the triclinic basis of the unit cell can be found in ref. 41. For this hierarchical lamellar morphology, two lengths of L_1 and L_2 are used to characterize the periodicity in two directions. In fact, the period of the morphologies except for the zero-shift one along the y direction is $2L_2$ because the two neighbor B/C-layers are distinguishable. The free energy of each structure is minimized by adjusting the box sizes L_x and L_y (or the two periods) carefully to ensure its high accuracy. For the 180-degree-shift morphology, the free energy is also minimized indirectly by the angle between the two basic vectors of the parallelogram because it is determined by the sizes of L_1 and L_2. We find that the two periods are hardly dependent on the shifting magnitude when the compositions and interactions of the copolymer are fixed. In Figure 1, their periods are $L_1 \approx 2.533\, R_g$ and $L_2 \approx 4.265\, R_g$.

To show the symmetries of the morphologies in Figure 1, the Fourier spectrums $|\phi_k(\mathbf{q})|$ (k = A, B) are calculated, and are present in Figure 2. The radii of filled circles are proportional to their intensities. As the spectrum $|\phi_A(\mathbf{q})|$ is almost independent on the shift angle of the morphology, only that of zero-shift is given in Figure 2(a). The spectrum plot suggests that it is a typical lamellar morphology. The spectrums $|\phi_B(\mathbf{q})|$ of the morphologies with 0-, 45-, 90-, 135-, and 180-degree shifts, are shown in Figures 2(b–f), respectively. Obviously $|\phi_B(\mathbf{q})|$ vary as the shift angle varies. For the zero-shift morphology, the peak positions of the Fourier spectrum indicate that the unit cell is a rectangle of (L_1, L_2) which is consistent with the density plots in Figure 1. When the shift angle increases from zero, the basic vector becomes $(L_1, 2L_2)$ from (L_1, L_2), and the unit cell contains two distinguishable grid points. The apostrophe on the digits is used to distinguish the crystal faces from those in (b). There is a phase difference between the contributions from the two points to the spectrums. The multiple factor induced by the phase difference is proportional to $|\cos[(h\theta + k\pi)/2]|$ when $\mathbf{q} = (2h\pi/L_1, 2k\pi/2L_2)$, where θ is the shift angle, and h and k are the indices of the crystal face. With the expression of the multiple factor, the intensities of these peaks in the spectrum plots from (c) to (f) can be understood readily. In Figure 2(c), the peak of $1'1'$ appears with a weak intensity determined by the factor of $|\cos[(\pi/4 + \pi)/2]| \approx 0.383$, and the peak of $1'0'$ has a decay compared with that of Figure 2(b). When θ increases to be 90 degrees, the peak intensity of $1'1'$ is comparable with that of $1'0'$ in Figure 2(d). And, eventually, the

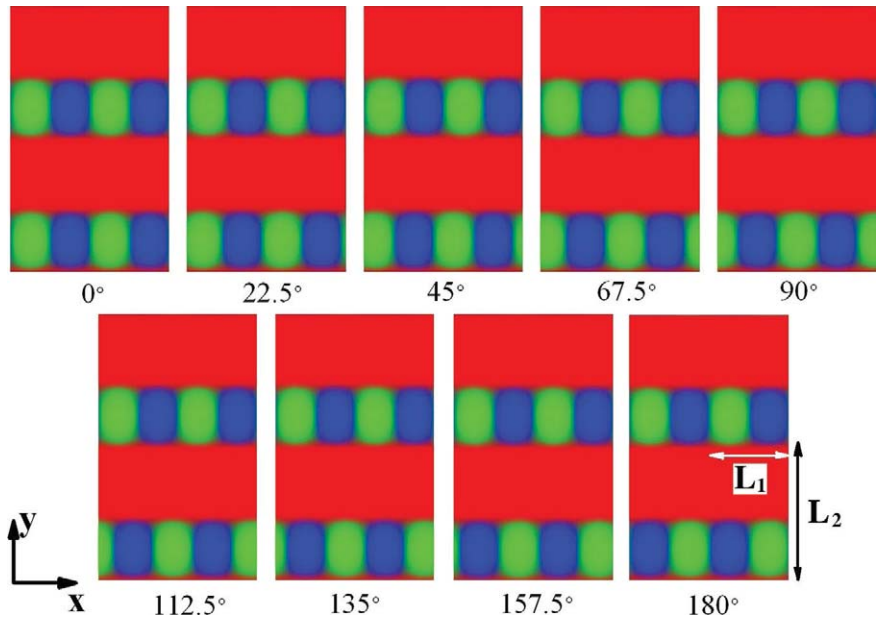

FIGURE 1 Monomer density plots of hierarchical lamellar morphologies with various shifts for $f_A = 0.6$ and $f_B = f_C = 0.2$. The colors of red, green and blue, indicate the regions where the most component is A, B, and C, respectively. The lamellae are aligned along the box side on the x direction, and the other side of the box is set on the y direction. On the density profile of 180-degree, the repeat spacing of B/C domains is denoted as L_1, and the distance between two neighbor layers is characterized by L_2. The two lengths L_1 and L_2 of the morphology are hardly dependent on the shifting magnitude. The shift is refered to an angle varying from 0 (none shift) to 180 degrees (the largest shift, or the shift of $L_1/2$). The morphologies of shift angles, 0, 22.5,..., 180 degrees, are shown.

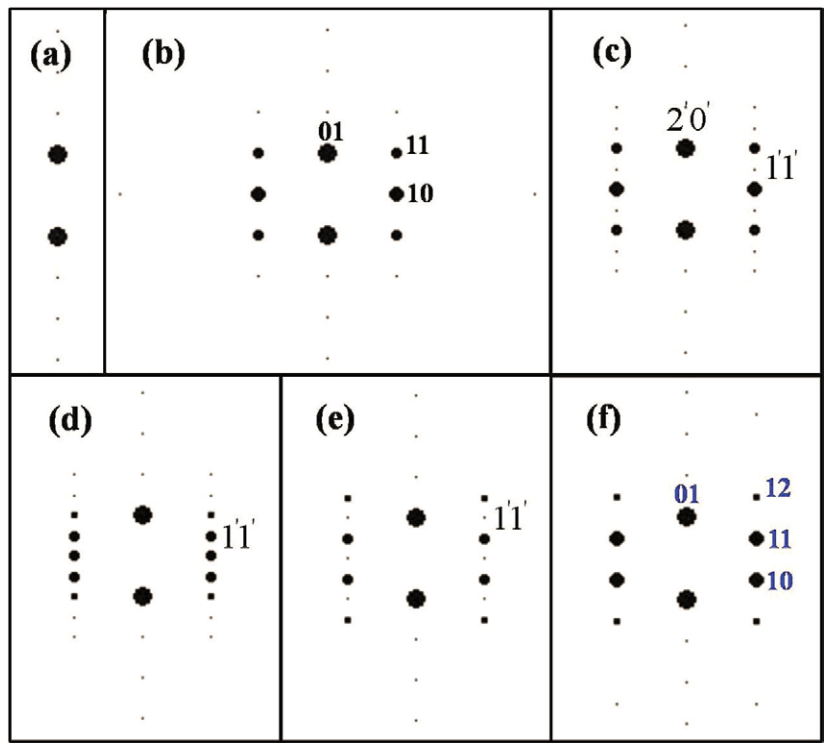

FIGURE 2 (a) The typical Fourier spectrum of the densities $\phi_A(\boldsymbol{r})$, which is almost independent on the shift angle of the morphology. The pictures from (b) to (f) are the Fourier spectrums of the density profiles $\phi_B(\boldsymbol{r})$ of the morphologies with shift angles of 0, 45, 90, 135, 180 degrees, respectively.

peak of 1′0′ disappears when $\theta = 180°$ in Figure 2(f). And accordingly, the unit cell has changed to be a parallelogram.

As the free energy of the morphology varying on the shift, a free energy difference, defined as the value of the free energy of a morphology subtracted by that of the 180-degree morphology, ΔF, is used to identify the relative stability among these morphologies for the reason of more intuitional than the free energy itself. The free energy of these morphologies in Figure 1 together with their differences to that of the 180-degree morphology for $\chi_{AB}N = \chi_{AC}N = \chi_{BC}N = 60$ are present in Table 1. We can see that the free energy difference is as tiny as 10^{-7}. This suggests that the value of the free energy difference is possible smaller than the accuracy of free energy in the real-space numberical SCMFT calculations. So it is neccessary to check the reliability of the data of the free energy difference. As we know, the discretization on the chain contour length is the main factor influencing the accuracy of the free energy compared with the discretization on the real space.[40] In this work, a lattice of 128×128 is used for the real space. In our calculations, we find that the free energy changes much less when we enlarge the lattice to be 256×256 than that induced by the increasing of the discretization from $N_s = 500$ to 2000. Therefore we focus our attention on the influence of N_s on the free energy difference. A rigorous method is to calculate the free energy of each morphology for a series of N_s, and then to predict the free energy F_∞ of $N_s = \infty$ by doing extrapolation. Finally, with the values of F_∞ of these morphologies, we can compute the free energy difference without the influence of the discretization N_s. In practice, this method is very time-consuming. Here two simpler ways are used to estimate the reliability of our results. One way is to increase $N_s = 500$ to 2000 for the OpS2 scheme to see how big the change of the free energy and the change of the difference are. Table 1 shows that the absolute value of the free energy changes significantly, but that of all morphologies has a similar increment of 6.6×10^{-4}. The free energy difference is hardly influenced for all morphologies though the increment is much bigger than it. The other way is to use the BDF4 scheme with higher accuracy for the same value of N_s. We calculate the free energy of morphologies with $N_s = 2000$ (see Table 1). Our results show that the discrepancy of the free energy between OpS2 and BDF4 for $N_s = 2000$ is about 4.4×10^{-5}, and the change of the free energy difference is negligible, too. Furthermore, we also do the similar checks for another group of interactions, $\chi_{AB}N = \chi_{AC}N = 40$, and $\chi_{BC} = 60$. The absolute value of the free energy have the similar tendency as that of $\chi_{AB}N = \chi_{AC}N = \chi_{BC}N = 60$ for three cases: $N_s = 500$ (OpS2), $N_s = 2000$ (OpS2), and $N_s = 2000$ (BDF4). Though the free energy difference, becomes much bigger (order of 10^{-5}), its error is still small. The above discussions suggest that the free energy difference obtained by the OpS2 method with $N_s = 500$ are reliable. To reduce the computing time, the OpS2 method with $N_s = 500$ is applied for all of other calculations in this work.

For the reason of visualization, the free energy differences as a function of the shift angle for $\chi_{AB}N = \chi_{AC}N = 60$ and $\chi_{AB}N = \chi_{AC}N = 40$ with the same $\chi_{BC}N = 60$ are plotted in Figure 3(a,b), respectively. That these symbols of the three cases are almost overlapped proves that the results obtained by $N_s = 500$ (OpS2) are reliable, too. In addition, the curves of $\Delta F/nk_BT$ are a consistent function without obvious stochastic errors. For $\chi_{AB}N = \chi_{AC}N = \chi_{BC}N = 60$, there are two properties with the curve. One property is that the free energy has difference as tiny as an order of 10^{-7} among these morphologies with various shifts. The other is that there are three extrema on the curve, and the minimal point is located at neither zero nor 180-degree shift, but at around 112.5-degree shift. This means that the stable morphology with a special shift angle between zero and 180 degrees is noncentrosymmetric. For $\chi_{AB}N = \chi_{AC}N = 40$, the magnitude of the difference increases to be an order of 10^{-5}. We can find a common characteristic from the two figures that the morphology with 180-degree shift has lower free energy than that with zero shift. However, the number of extrema decreases to be two in Figure 3(b). This tells us that the morphology with 180-degree shift is stable instead of that with an about 112.5-degree shift in Figure 3(a). The comparison of the two figures reveals that the interaction parameters of χ_{AB} and χ_{AC} influence the free energy differences among these morphologies with various shifts, and therefore change their relative stabilities.

TABLE 1 The Data of Free Energy Obtained by Two Numerical Schemes of OpS2 and BDF4 for $\chi_{AB}N = \chi_{AC}N = \chi_{BC}N = 60$

Shift	$\frac{\Delta F}{nk_BT}$ ($\times 10^{-7}$) OpS2 $N_s = 500$	$\frac{\Delta F}{nk_BT}$ ($\times 10^{-7}$) OpS2 $N_s = 2000$	$\frac{\Delta F}{nk_BT}$ ($\times 10^{-7}$) BDF4 $N_s = 2000$	$\frac{F}{nk_BT}$ OpS2 $N_s = 500$	$\frac{F}{nk_BT}$ OpS2 $N_s = 2000$	$\frac{F}{nk_BT}$ BDF4 $N_s = 2000$
0	6.99	6.99	7.00	11.017270602	11.017928162	11.017972663
22.5	5.99	5.99	6.00	11.017270502	11.017928062	11.017972563
45	3.49	3.48	3.50	11.017270252	11.017927811	11.017972313
67.5	0.62	0.62	0.63	11.017269965	11.017927525	11.017972026
90	−1.43	−1.43	−1.42	11.017269760	11.017927320	11.017971821
112.5	−2.05	−2.05	−2.04	11.017269698	11.017927258	11.017971759
135	−1.45	−1.45	−1.44	11.017269758	11.017927318	11.017971819
157.5	−0.46	−0.46	−0.46	11.017269857	11.017927417	11.017971917
180	0	0	0	11.017269903	11.017927463	11.017971963

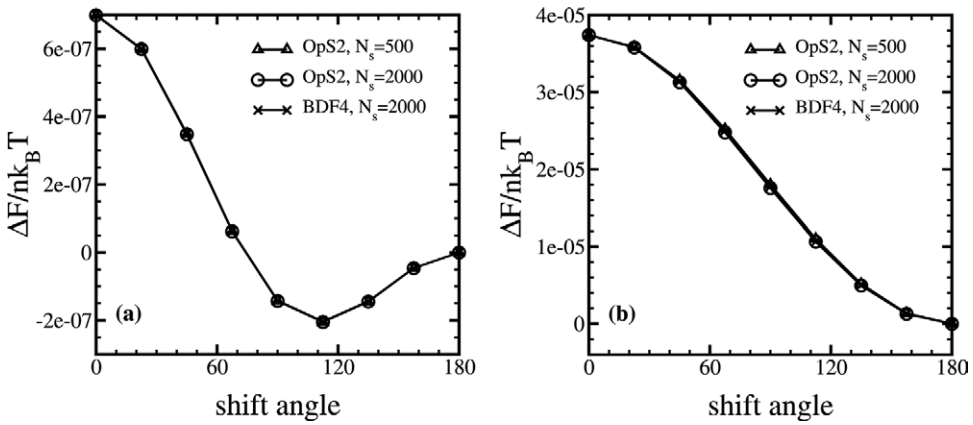

FIGURE 3 The free energy difference as a function of the shift angle (a) for $\chi_{AB}N = \chi_{AC}N = \chi_{BC}N = 60$ (same as Table 1); (b) for $\chi_{AB}N = \chi_{AC}N = 40$, and $\chi_{BC}N = 60$. The connected lines are guides to the eye.

To understand the dependence of the free energy on the shift, we seperate the free energy into two parts: internal (U) and entropic ($-TS$). The internal and entropic contributions to the free energy can be expressed as[8]

$$\begin{aligned}\frac{U}{nk_BT} &= \frac{1}{V}\int d\mathbf{r}\big[\chi_{AB}N\phi_A(\mathbf{r})\phi_B(\mathbf{r}) \\ &\quad + \chi_{AC}N\phi_A(\mathbf{r})\phi_C(\mathbf{r}) + \chi_{BC}N\phi_B(\mathbf{r})\phi_C(\mathbf{r})\big] \\ -\frac{S}{nk_B} &= -\ln Q - \frac{1}{V}\int d\mathbf{r}\big[\omega_A(\mathbf{r})\phi_A(\mathbf{r}) \\ &\quad + \omega_B(\mathbf{r})\phi_B(\mathbf{r}) + \omega_C(\mathbf{r})\phi_C(\mathbf{r})\big]. \end{aligned} \quad (5)$$

ΔU and $-T\Delta S$, the corresponding parts of the free energy difference, are shown in Figure 4 together with ΔF. The two figures reveal that the morphology with smaller shift has lower internal energy but higher entropic energy. The lower internal energy for smaller shift can be interpreted by the weak interfacial energy between two neighbor B/C-domain layers as they are separated by an A-domain layer. The interfacial energy becomes weaker when B (or C) domains in one layer face same B (or C) domains in its neighbor layers. So small-shift morphology is favored by the contribution of the internal energy. On the other hand, the entropic energy becomes higher for smaller-shift morphology. It is known that the entropic contribution is mainly from the chain stretching which is usually attributed to the domain sizes. However our calculations suggest that the domain sizes are almost independent on the magnitude of the shift for fixed interaction parameters. It means that the difference of entropic energy is from a secondary contribution. The competition between the two factors, which have opposite tendency for varying shift, determines the relative stability of these morphologies. In Figure 4(b), as the entropic energy dominates the free energy over the whole range of the shift, the morphology with the largest shift of 180-degree is stable. In Figure 4(a), the dominance of the entropic contribution over the internal contribution is reduced by increased value of $\chi_{AB} = \chi_{AC}$. The combination of the two contributions leads to a stable morphology with an about 112.5-degree shift.

According to the discussions, we can see the free energy difference as a secondary effective interaction between two neighboring B/C-layers. The dependence of the free energy

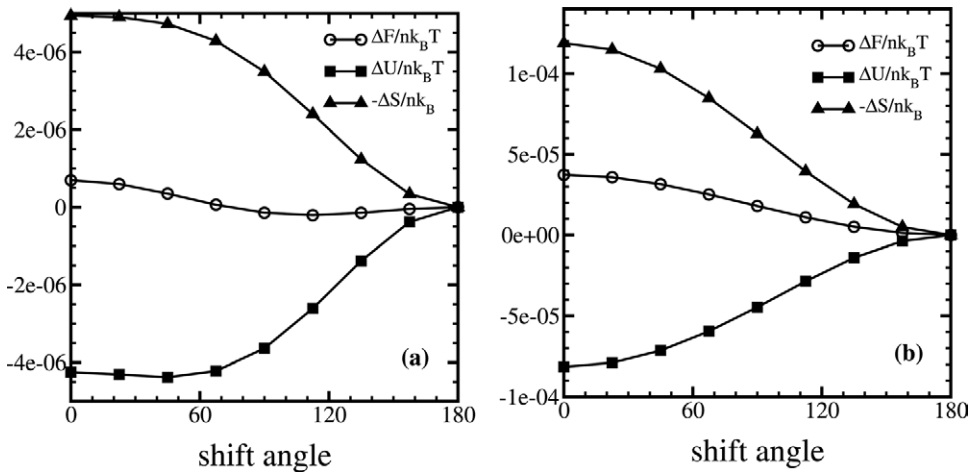

FIGURE 4 The internal and entropic parts of the free energy difference as well as itself as a function of the shift angle for (a) $\chi_{AB}N = \chi_{AC}N = \chi_{BC}N = 60$; and (b) $\chi_{AB}N = \chi_{AC}N = 40$, and $\chi_{BC}N = 60$.

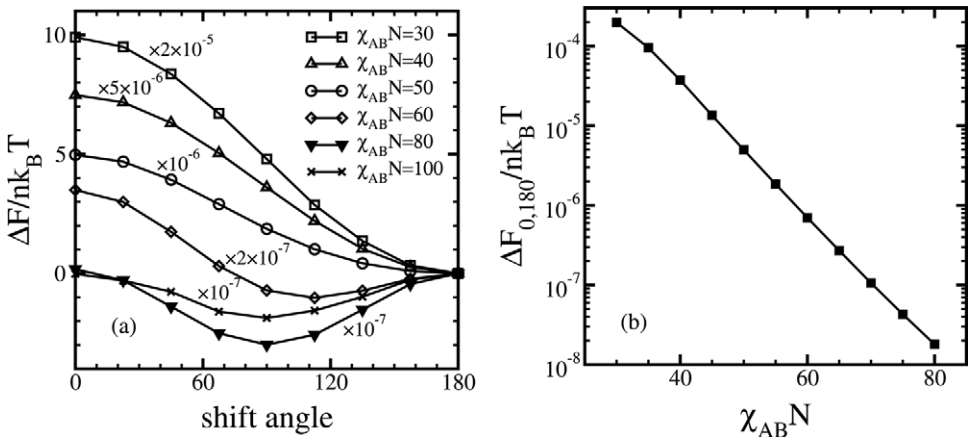

FIGURE 5 (a) The free energy difference as a function with respect to varying shift angles for $\chi_{AB}N = \chi_{AC}N = 30, 40, 50, 60, 80, 100$ and fixed $\chi_{BC}N = 60$. (b) The free energy difference between the two morphologies of zero shift and 180-degree shift, $\Delta F_{0,180}/nk_BT$, for various values of $\chi_{AB}N = \chi_{AC}N$.

difference on the interactions of $\chi_{AB} = \chi_{AC}$ can be explained by the change of the interacting distance between two neighbor B/C-layers. Because the interfacial areas between A and B/C domains are decreased to reduce interfacial energy resulted by increased $\chi_{AB} = \chi_{AC}$, the interaction distance between two B/C-layers, that is, the domain size on the direction perpendicular to the lamellae, is increased. In consequence, the effective interaction is weakened by the increased interacting distance. To show the effect more systematically, the free energy difference of a few groups of parameters $\chi_{AB}N = \chi_{AC}N$ for fixed $\chi_{BC}N = 60$ are calculated. In Figure 5(a), the curves of the free energy difference are drawn for $\chi_{AB}N = \chi_{AC}N =$ 30, 40, 50, 60, 80, 100. For the reason of clarity , the data of $\Delta F/nk_BT$ are divided by various constants, 2×10^{-5}, 5×10^{-6}, 10^{-6}, 2×10^{-7}, 10^{-7}, and 10^{-7}, respectively. When $\chi_{AB}N = \chi_{AC}N$ is increased from 60 to 80, the shift angle of the stable morphology goes down from about 112.5 degrees to about 90 degrees. When $\chi_{AB}N = \chi_{AC}N$ is increased further to be 100, the shift angle of the stable morphology stays at around 90 degrees, but the magnitude of ΔF becomes smaller. Actually, for $\chi_{AB}N = \chi_{AC}N = 80$ and 100, the values of ΔF are very small. However, when $\chi_{AB}N = \chi_{AC}N$ is decreased, three-extremum curves become two-extremum ones with the minimum at 180-degree shift, and the magnitude of ΔF continuously increases to the order of 10^{-4} for $\chi_{AB}N = \chi_{AC}N = 30$. To gain a quantitative picture of the magnitude, we introduce a quantity, $\Delta F_{0,180}/nk_BT$ defined as the free energy difference between the two morphologies with zero shift and 180-degree shift, to do this measurement. The logarithm of $\Delta F_{0,180}/nk_BT$ is shown for from $\chi_{AB}N = \chi_{AC}N = 30$ to 80 in Figure 5(b). The good linear relation tells us that the magnitude of $\Delta F_{0,180}/nk_BT$ decreases exponentially over the examined range of $\chi_{AB}N = \chi_{AC}N \lesssim 80$. The expoenential tendency predicts that the free energy difference has become very tiny when $\chi_{AB}N = \chi_{AC}N = 100$. In fact, the data of $\Delta F_{0,180}/nk_BT$ is negative with a absolute value smaller than 10^{-9}. In another word, the morphologies with various shifts become indistinguishable if the free energy difference vanishes.

After examining how the value of $\chi_{AB}N = \chi_{AC}N$ influences the dependence of relative stability of the morphology on the shift angle, we turn to study the influence of varied $\chi_{BC}N$ by fixing $\chi_{AB}N = \chi_{AC}N$. Similarly, the free energy differences with various shifts are present for $\chi_{BC}N = 40$, 50, 60, 70, 80 when $\chi_{AB}N = \chi_{AC}N$ is fixed as 40 in Figure 6(a), and $\Delta F_{0,180}/nk_BT$ as

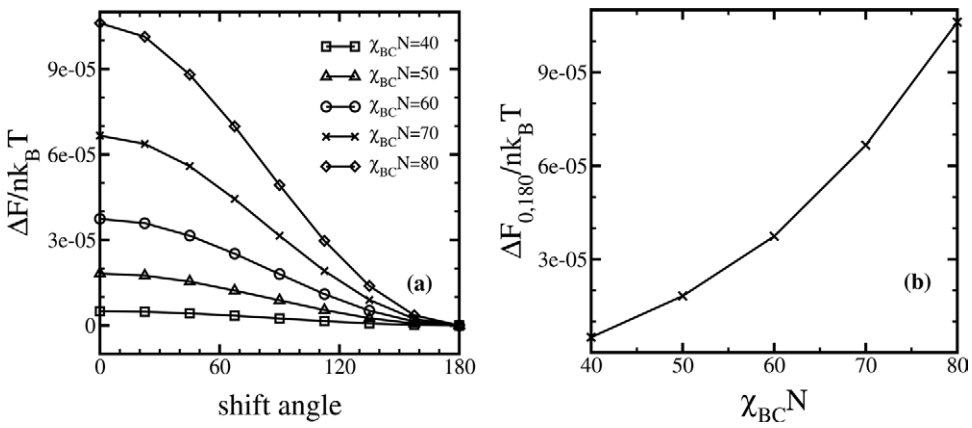

FIGURE 6 (a) The free energy difference as a function of the shift angle for $\chi_{BC}N = 40, 50, 60, 70, 80$, and fixed $\chi_{AB}N = \chi_{AC}N = 40$. (b) The free energy difference between the two morphologies of zero shift and 180-degree shift, $\Delta F_{0,180}/nk_BT$, as a function of $\chi_{BC}N$.

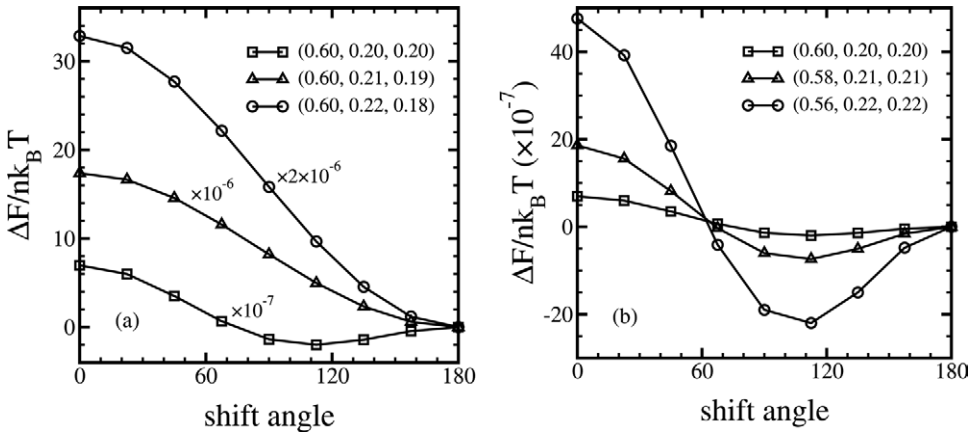

FIGURE 7 The free energy difference as a function of the shift angle for different compositions and fixed $\chi_{AB}N = \chi_{AC}N = \chi_{BC}N = 60$. (a) The A composition is fixed as $f_A = 0.60$, and two asymmetric compositions of B and C, $(f_B,\ f_C) = (0.21,\ 0.19)$ and $(f_B,\ f_C) = (0.22,\ 0.18)$, are considered. (b) The asymmetry of B and C blocks is kept, and the compositions are $(f_B,\ f_C) = (0.21,\ 0.21)$ and $(f_B,\ f_C) = (0.22,\ 0.22)$. As comparisons, the data of $f_A = 0.6$ and $f_B = f_C = 0.2$ is shown in both (a) and (b).

a function of $\chi_{BC}N$ is present in Figure 6(b). In this series of results, the morphology with 180-degree shift has always the relative stability upon other morphologies, and $\Delta F_{0,180}/nk_BT$ increases as $\chi_{BC}N$ increasing for fixed $\chi_{AB}N = \chi_{AC}N$. When we compare the $\Delta F/nk_BT$ curve of $\chi_{AB}N = \chi_{AC}N = \chi_{BC}N = 40$ with that of $\chi_{AB}N = \chi_{AC}N = \chi_{BC}N = 60$ in Figure 3(a), we find that the global minimum, which is located at about 112.5-degree shift in the latter case, dispears in the former case. For gaussian polymer chains, the entropic contribution usually becomes more dominant over the internal interaction when the interaction parameters decreases or when the temperature increases. For $\chi_{AB}N = \chi_{AC}N = \chi_{BC}N = 40$, the internal interaction, with an opposite changing tendency to the entropic energy for varied shift, is too weak to make the free energy difference have another minimum besides that one at the 180-degree shift. When $\chi_{BC}N$ is increased for fixed $\chi_{AB}N = \chi_{AC}N = 40$, the stronger interaction between B and C blocks induces the B/C domains along the direction of the lamellar alignment (or x direction) to be stretched to reduce the B/C interfacial energy, and as a consequence, the A-domain layer is compressed because of the conserved volume per chain. Larger interacting area per chain and shorter interacting distance result in a larger effective interaction. This is the reason that $\Delta F_{0,180}/nk_BT$ increases as $\chi_{BC}N$ increasing for fixed $\chi_{AB}N = \chi_{AC}N$.

In the above paragraphs, the compositions of the three components are fixed as $f_A = 0.6$ and $f_B = f_C = 0.2$. Now we consider the relative stability of the morphology for different compositions. To keep the hierarchical lamellae as equilibrium phase, we vary the compositions slightly by two ways. One way is to introduce a small asymmetry to B/C blocks when fixing $f_A = 0.6$. Two group of volume fractions, $(f_B,\ f_C) = (0.21,\ 0.19)$ and $(f_B,\ f_C) = (0.22,\ 0.18)$ are considered in our study. The other way is to change the A composition when keeping the symmetry between B and C blocks. The free energy differences in the two cases for $\chi_{AB}N = \chi_{AC}N = \chi_{BC}N = 60$ are plotted in Figure 7(a) and (b), respectively. In Figure 7(a), the three-extremum curve is changed to be the two-extremum curves by the introduction of the small asymmetry of the composition, and the magnitude of the free energy difference is increased significantly. During the phase separation between B/C blocks, the composition asymmetry induces a spontaneous curvature which is unfavorable for chain stretching. In subsequence, the B/C domain size is increased, and the A-layer width is decreased for the volume-conservation reason. The increased interacting area and decreased interacting distance account for the increment of the magnitude of the free energy difference. In Figure 7(b), $\Delta F/nk_BT$ for the compositions of $(f_B,\ f_C) = (0.21,\ 0.21)$ and $(f_B,\ f_C) = (0.22,\ 0.22)$ as well as $(f_B,\ f_C) = (0.20,\ 0.20)$ are shown. It is revealed that the increasing of B and C blocks changes hardly the minimal position, but amplifies the magnitude of the whole curve. The two results in Figure 7(a,b) indicate that existence of the minimum between zero and 180-degree shift is very sensitive to the symmetry of the composition of the copolymer.

CONCLUSIONS

To summarize, we have studied the relative stability of the hierarchical lamellar morphologies with various shifts formed in ABC star triblock copolymers with $f_A = 0.6$, and $f_B = f_C = 0.2$. In general, the morphology with the largest shift (or 180-degree) is the stable phase, and the free energy difference among these morphologies with various shifts is very small, especially when the interaction parameters satisfy the condition of $\chi_{AB}N = \chi_{AC}N \geq \chi_{BC}N$. The stable morphology with a shift different from the 180-degree has been observed in this condition, such as, about 112.5-degree for $\chi_{AB}N = \chi_{AC}N = \chi_{BC}N = 60$, 90-degree for $\chi_{AB}N = \chi_{AC}N = 80$ (or 100) and $\chi_{BC}N = 60$. The morphologies with zero and 180-degree shifts are centrosymmetric, whereas the others are noncentrosymmetric. The magnitude of the free energy difference between the two morphologies with zero shift and 180-degree shift, $\Delta F_{0,180}/nk_BT$, increases exponentially as $\chi_{AB}N = \chi_{AC}N$ decreasing for fixed $\chi_{BC}N$. It can vary over a range of a few orders. Varying of $\chi_{BC}N$ for fixed $\chi_{AB}N = \chi_{AC}N$ can influence significantly the value of $\Delta F_{0,180}/nk_BT$, too. However, the varying

magnitude is much smaller. We have also investigated the influencing of the three compositions on the relative stability of these morphologies. Our results predict that it is more possible to observe the morphology with 180-degree shift in experiments as an exact symmetric composition is hard to be obtained.

The star triblock copolymers have complex self-assembling behaviors in bulk. Our careful calculations and analysis can help us to understand the factors which influence the stability of the hierarchical lamellae in theory. Though many experiments have been carried to study their structure formations, the observation of this hierarchical lamellae is still lacking in neat star triblock copolymers. It is hoped that our theoretical predictions can be taken as a motivation to search these different lamellae.

The authors grateful to E. W. Cochran for helping them with the fourth-order scheme and to Q. Wang for useful discussions. This work was supported by the National Natural Science Foundation of China (Grants 20974026, 20990231, 20625413). W. L. gratefully acknowledges the support from Shanghai Pujiang Program (Programs No. 08PJ1402000), the Shanghai Educational Development Foundation, and the Scientific Research Foundation for the returned Overseas Chinese Scholars, State Education Ministry.

REFERENCES AND NOTES

1 Park, C.; Yoon, J.; Thomas, E. L. Polymer 2003, 44, 6725–6760.

2 Bates, F. S.; Schulz, M. F.; Khandpur, A. K.; Förster, S.; Rosedale, J. H.; Almdal, K.; Mortensen, K. Faraday Discuss 1994, 98, 7–18.

3 Föster, S.; Khandpur, A. K.; Zhao, J.; Bates, F. S.; Hamley, I. W.; Ryan, A. J.; Bras, W. Macromolecules 1994, 27, 6922–6935.

4 Khandpur, A. K.; Förster, S.; Bates, F. S.; Hamley, I. W.; Ryan, A. J.; Bras, W.; Almdal, K., Mortensen, K. Macromolecules 1995, 28, 8796–8806.

5 Leibler, L. Macromolecules 1980, 13, 1602–1617.

6 Matsen, M. W.; Schick, M. Phys Rev Lett 1994, 72, 2660–2663.

7 Drolet, F.; Fredrickson, G. H. Phys Rev Lett 1999, 83, 4317–4320.

8 Matsen, M. W. J Phys Condens Matter 2002, 14, R21–R47.

9 Tyler, C. A.; Morse, D. C. Phys Rev Lett 2005, 94, 208302.

10 Tyler, C. A.; Qin, J.; Bates, F. S.; Morse, D. C. Macromolecules 2007, 40, 4654–4668.

11 Hadjichristidis N.; Iatrou, H.; Behal, S. K.; Chludzinski, J. J.; Disko, M. M.; Carner, R. T.; Liang, K. S.; Lohse, D. J.; Milner, S. T. Macromolecules 1993, 26, 5812–5815.

12 Hückstädt, H.; Abetz, V.; Stadler, R. Macromol Rapid Commun 1996, 17, 599–606.

13 Okamoto, S.; Hasegawa, H.; Hashimoto, T.; Fujimoto, T.; Zhang, H.; Kazama, T.; Takano, A. Polymer 1997, 38, 5275–5281.

14 Sioula, S.; Tselikas, Y.; Hadjichristidis, N. Macromolecules 1997, 30, 1518–1520.

15 Sioula, S.; Hadjichristidis, N.; Thomas, E. L. Macromolecules 1998, 31, 5272–5277; 1998, 31, 8429–8432.

16 Hückstädt, H.; Gopfert, A.; Abetz, V. Macromol Chem Phys 2000, 201, 296–307.

17 Yamauchi, K.; Takahashi, K.; Hasegawa, H.; Iatrou, H.; Hadjichirstidis, N.; Kaneko, T.; Nishikawa, Y.; Jinnai, H.; Matsui, T.; Nishioka, H.; Shimizu, M.; Furukawa, H. Macromolecules 2003, 36, 6962-6966.

18 Takano, A.; Wada, S.; Sato, S.; Araki, T.; Hirahara, K.; Kazama, T.; Kawahara, S.; Isono, Y.; Ohno, A.; Tanaka, N.; Matsushita, Y. Macromolecules 2004, 37, 9941–9946.

19 Yamauchi, K.; Akasaka, S.; Hasegawa, H.; Iatrou, H.; Hadjichristidis, N. Macromolecules 2005, 38, 8022–8027.

20 Takano, A.; Kawashima, W.; Noro, A.; Isono, Y.; Tanaka, N.; Dotera, T.; Matsushita, Y. J Polym Sci Part B: Polym Phys 2005, 43, 2427–2432.

21 Hayashida, K.; Kawashima, W.; Takano, A.; Shinokara, Y.; Amemiya, Y.; Nozue, Y.; Matsushita, Y. Macromolecules 2006, 39, 4869–4872.

22 Hayashida, K.; Saito, N.; Arai, S.; Takano, A.; Tanaka, N.; Matsushita, Y. Macromolecules 2007, 40, 3695–3699.

23 Hayashida, K.; Dotera, T.; Takano, A.; Matsushita, Y. Phys Rev Lett 2007, 98, 195502.

24 Iatrou, H.; Hadjichristidis, N. Macromolecules 1992, 25, 4649–4651.

25 Fujimoto, T.; Zhang, H.; Kazanawa, H.; Isono, X.; Hasegawa, H.; Hashimoto, T. Polymer 1992, 33, 2208–2213.

26 Gemma, T.; Hatano, A.; Dotera, T. Macromolecules 2002, 35, 3225–3237.

27 Matsushita, Y. Macromolecules 2007, 40, 771–776.

28 Huang, C. I.; Fang, H. K.; Lin, C. H. Phys Rev E 2008, 77, 031804.

29 Xu, Y. C.; Li, W. H.; Qiu, F.; Yang, Y. L.; Shi, A. C. J Phys Chem B 2009, 113, 11153–11159.

30 Tang, P.; Qiu, F.; Zhang, H.; Yang, Y. J Phys Chem B 2004, 108, 8434–8438.

31 Bohbot-Raviv, Y.; Wang, Z. G. Phys Rev Lett 2000, 85, 3428–3431.

32 Kou, D. Z.; Jiang, Y.; Liang, H. J. J Chem Phys 2006, 110, 23557–23563.

33 Shi, A.-C. In Development in Block Copolymer Science and Technology; Hamley, I. W., Ed.; Wiley: New York, 2004.

34 Fredrickson, G. H. The Equilibrium Theory of Inhomogeneous Polymers; Oxford University Press: Oxford, 2006.

35 Helfand, E. J Chem Phys 1975, 62, 999–1005.

36 Hong, K. M.; Noolandi, J. Macromolecules 1981, 14, 727–736.

37 Guo, Z.; Zhang, G.; Qiu, F.; Zhang, H.; Yang, Y.; Shi, A.-C. Phys Rev Lett 2008, 101, 028301.

38 Tzeremes, G.; Rasmussen, K. Ø; Lookman, T.; Saxena, A. Phys Rev E 2002, 65, 041806.

39 Rasmussen, K. Ø.; Kalosakas, G. J. J Polym Sci Part B: Polym Phys 2002, 40, 1777–1783.

40 Cochran, E. W.; Garcia-Cervera, C. J.; Fredrickson, G. H. Macromolecules 2006, 39, 2449–2451.

41 Kriksin, Y. A.; Erukhimovich, I. Y.; Khalatur, P. G.; Smirnova, Y. G.; ten Brinke, G. J Chem Phys 2008, 128, 244903.